ANALYSIS OF RE-LIQUEFACTION PROPERTIES BASED ON ENERGY APPROACH

Seto WAHYUDI[1] and Junichi KOSEKI[2]

ABSTRACT: Analysis of re-liquefaction properties of Toyoura sand based on dissipated energy is conducted on results from a series of constant-volume cyclic torsional shear tests using stacked-ring shear apparatus. During liquefaction, dissipated energy accumulated at different rates depending on the current effective stress states before/after passing the phase transformation line as well as reaching the zero effective stress state. The amount of dissipated energy in the previous liquefaction stage affected both positively and negatively the behavior in the next liquefaction stage. A positive impact of dissipated energy accumulated first, while a negative impact of dissipated energy prevailed later. Compilation of the re-liquefaction test results revealed a unique relationship among the amounts of the positive and negative impacts of dissipated energy that accumulated in the previous liquefaction stage and the liquefaction resistance to be mobilized in the next stage.

Key Words: re-liquefaction, stacked-ring shear apparatus, dissipated energy, strain amplitude, phase transformation

INTRODUCTION

In order to investigate the re-liquefaction properties of Toyoura sand, analysis of dissipated energy is conducted on results from a series of constant-volume cyclic torsional shear tests subjected to various strain amplitudes using stacked-ring shear apparatus. Details of the test apparatus and some of the preliminary test results have been reported by Wahyudi et al. (2014), while further modification of the apparatus has been made by applying a special coating, called Diamond Like Coating, to the stacked-rings in order to reduce as much as possible the friction mobilized at the interface between the rings and the specimen.

TESTING APPARATUS

A newly developed ring shear testing device as shown in Fig. 1a, called herein as stacked-ring shear apparatus, was employed to study the re-liquefaction behavior. As shown in Figs. 1b and 1c, lateral deformation of a hollow cylindrical specimen is constrained by using two sets of eleven pieces of vertically-stacked donut-shape metal rings. The specimen has a height of 5.5 cm, outer diameter of 15 cm and inner diameter of 9 cm, on which torsional torque and vertical load are applied through loading systems using a combination of a direct-drive motor and reduction gears, and a pair of bellofram cylinders, respectively.

A couple of bi-component load cells are installed to measure the torque and vertical load applied to the top and bottom of the specimen and to evaluate the friction mobilized at the interface between the specimen and the ring walls. By making a special coating, called Diamond Like Coating, on the ring

[1] Formerly PhD student, Dept. of Civil Engineering, The University of Tokyo
[2] Professor, Institute of Industrial Science, The University of Tokyo

walls, it was attempted to reduce the friction, while the friction angle mobilized at the interface in the vertical direction was about 20 degrees under the testing conditions employed in the current study. In this paper, the test results will be shown in terms of the stresses at the middle height of the specimen, by using the average values measured at the top and bottom of the specimen. Vertical and shear strains were measured by strain gauge-type displacement transducer and potentiometers, respectively. Further details of the apparatus development are provided in Wahyudi et al. (2014).

By using a clumping device to prevent vertical displacement of the loading shaft, a series of constant-volume cyclic torsional shear tests were executed in the current study. As typically shown in Figs. 2a through 2c, a state of zero vertical stress accompanied by a rapid increase in the shear strain amplitude was observed with an air-dried sand specimen. Since such behavior corresponds to the liquefaction of saturated sand specimen, it will be simply denoted as "liquefaction" in this paper. By taking advantage of the fact that the specimen shape can be maintained even after undergoing large shear deformation, multiple-liquefaction tests on single specimen were performed in the current study.

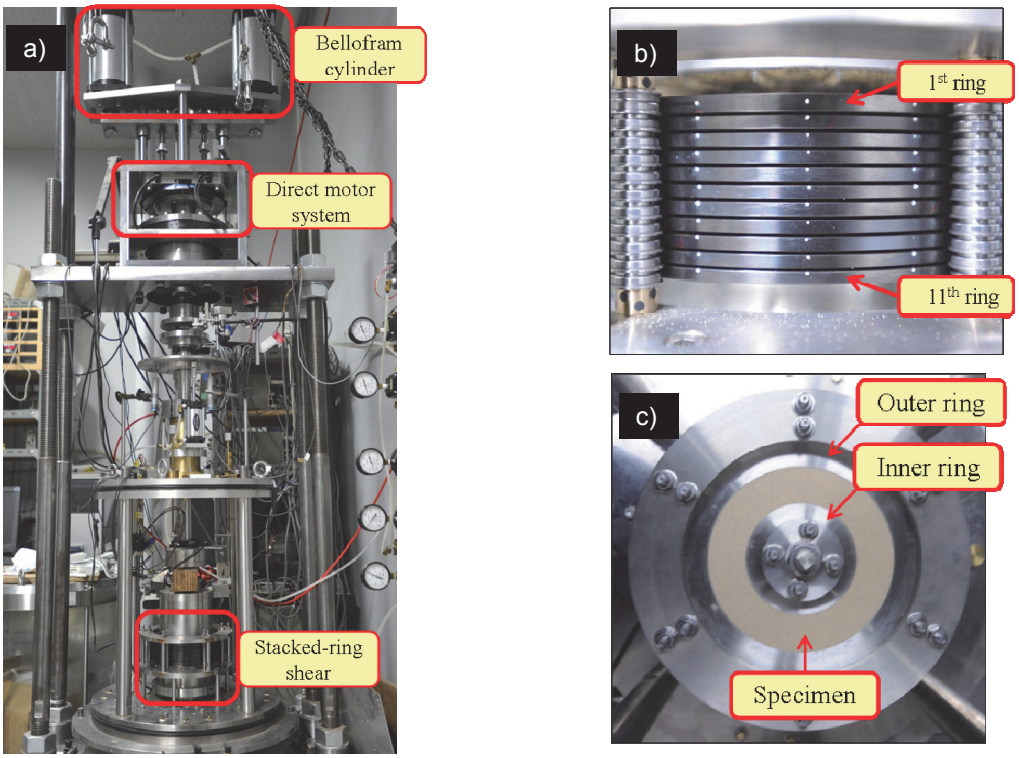

Figure 1. stacked-ring shear apparatus; a) general view, b) side view and c) plan view of stacked-rings

TEST MATERIAL AND PROCEDURES

Toyoura sand with a mean particle diameter (D_{50}) of about 0.19 mm was used as the testing material. It has particles angular to sub-angular in shape and the following physical properties: specific gravity, G_s = 2.656; fines content less than 75 μm, F_c = 0.1%; maximum void ratio, e_{max} = 0.992; and minimum void ratio, e_{min} = 0.632.

Specimens were prepared by the air pluviation method using air-dried sand particles. Multiple-liquefaction tests were conducted on specimens prepared at an initial relative density (D_{r0}) of about 52±2%. For comparison purpose, several single-stage liquefaction tests were also conducted on specimens prepared at different initial relative densities (D_{r0} = 51-74%).

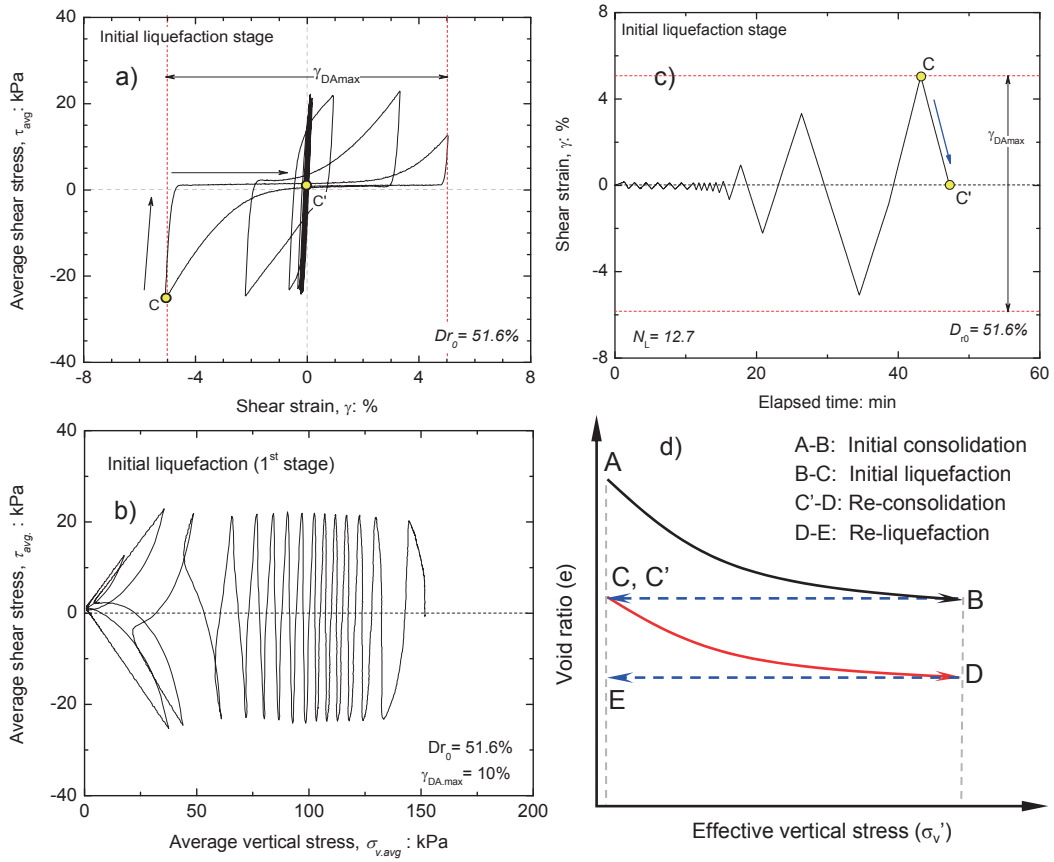

Figure 2. Typical test results; a) stress-strain relationship, b) effective stress path and c) time history of shear strain during first liquefaction stage, and d) schematic change in void ratio during multiple liquefaction and consolidation stages

The specimens were one-dimensionally consolidated by gradually increasing the effective vertical stress measured at the top of the specimen (σ_v'$_{top}$) up to 200 kPa, i.e. from state A to state B, as shown in Fig. 2d. Then, a cyclic shear stress (τ_{cyc}) of ±25 kPa was applied under constant-volume conditions. The cyclic loading was terminated when the double amplitude shear strain (γ_{DAmax}) reached a pre-fixed value in the range of 0.2 to 10.0 % (state C shown in Figs. 2a, 2c and 2d). Prior to this constant-volume cyclic loading stage, another cyclic loading stage was applied with "pre-sheared" specimens.

In conducting multiple-liquefaction tests, by adding unloading stage while keeping the constant-volume condition, the shear strain was resumed to be zero (state C' in Figs. 2a and 2c). In case of real liquefaction event with horizontal ground, not the shear strain but the shear stress shall be resumed to be zero. In the current study, however, the above process was employed to prevent possible additional effects of induced-anisotropy while investigating the effects of shear strain amplitude (Ishihara and Okada, 1978). The next liquefaction stage was then started by re-consolidating the liquefied specimens to the original effective vertical stress (σ_v'$_{top}$) up to 200 kPa at state D. Then, the subsequent liquefaction stages were continued by following the same procedure as those described for the first liquefaction stage.

At each liquefaction stage, the liquefaction resistance was evaluated as the number of cycles (N_L) needed to reach a γ_{DA} of 2%.

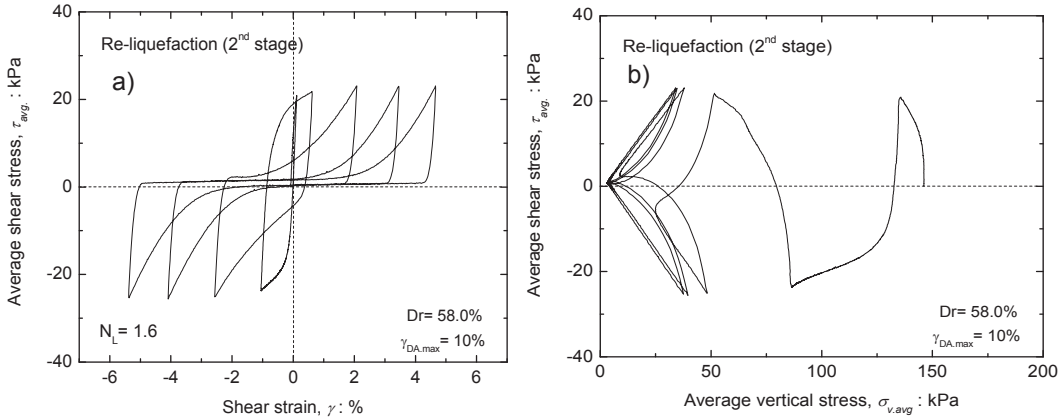

Figure 3. Typical test results; a) stress-strain relationship and b) effective stress path during second liquefaction stage

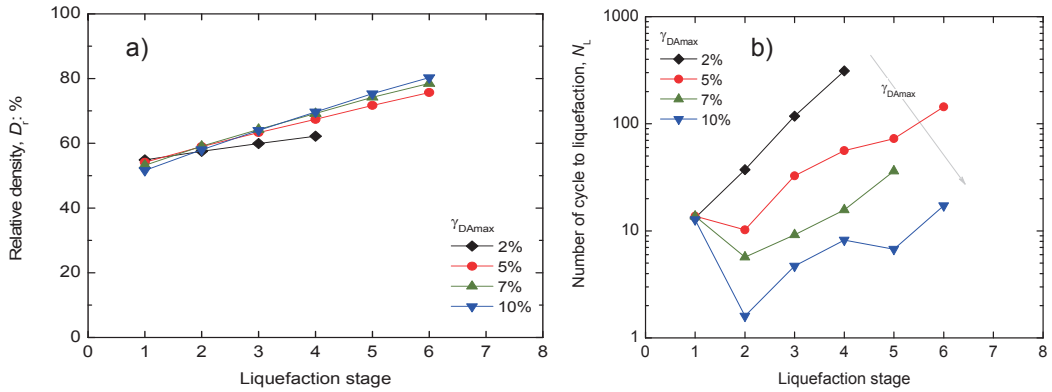

Figure 4. Summary of multiple-liquefaction test results; a) change in *D*r and b) change in N_L

TEST RESULTS

As typical re-liquefaction behavior of Toyoura sand, the results from the second liquefaction stage of the specimen which was subjected to γ_{DAmax} =10.0 % are shown in Fig. 3. In this particular case, as compared to the stress-strain relationship and the stress path during the first liquefaction stage as shown in Figs. 2a and 2b, reduction of the vertical stress induced by constant-volume cyclic shearing was much more significant, which was accompanied by earlier increase of shear strain amplitudes. As a result, the number of cycles to induce the double amplitude shear strain of 2 %, N_L, decreased to 1.6 in the second stage from 12.7 in the first stage. It should be noted that, due to the vertical compression of the specimen during the re-consolidation stage (from states C' to D shown in Fig. 1d), the relative density of the specimen, *D*r, increased from 51.6 % in the second stage to 58.0 % in the second stage.

A summary of the multiple-liquefaction test results conducted with γ_{DAmax} =2.0, 5.0, 7.0 and 10.0 % is made in Fig. 4. As shown in Fig. 4a, the *D*r value increased gradually with the liquefaction stage, while such densification was less pronounced in the test with γ_{DAmax} =2.0 % than in the other tests with larger γ_{DAmax} values. On the other hand, as shown in Fig. 4b, the N_L values in the second to fourth liquefaction stages were highest in the test with γ_{DAmax} =2.0 %, and they decreased with the increase in the γ_{DAmax} value. As a result of these changes, as shown in Fig. 5, the relationships between *D*r and N_L were different from each other depending on the γ_{DAmax} value.

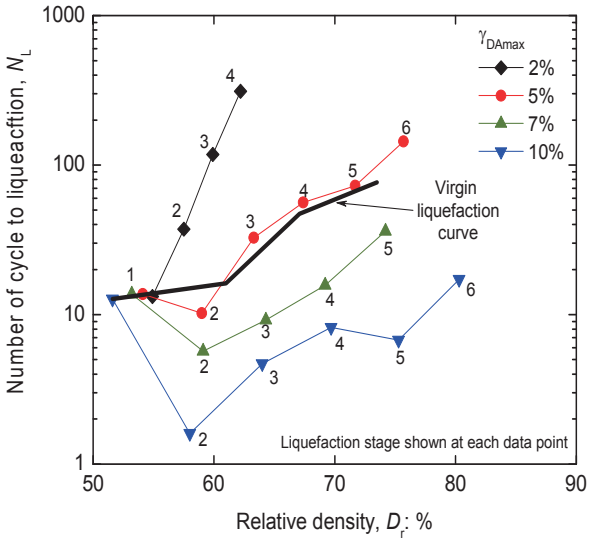

Figure 5. Relationships between *D*r and N_L in multiple-liquefaction and single-stage liquefaction tests

In Fig. 5, the relationship obtained from the single-stage liquefaction tests at different initial relative densities is also shown. In comparison with this relationship, the following trends of multiple-liquefaction behavior could be observed:

1) The specimen sheared up to γ_{DAmax} = 2.0 % always exhibits higher liquefaction resistance.
2) The specimen sheared up to γ_{DAmax} = 5.0 % has almost the same liquefaction resistance, except for the 2nd stage.
3) The specimens sheared up to $\gamma_{DA.max}$ = 7.0 % and 10.0 % have smaller liquefaction resistance.

The above observations suggest that the strain history in the preceding liquefaction stages affects significantly the liquefaction resistance to be mobilized in the next stage, which will be analyzed based on a view point of dissipated energy in the following section.

EVALUATION OF DISSIPATED ENERGY AND DISCUSSIONS

Relationships between dissipated energy and accumulated strain

As illustrated in Fig. 6a, the energy ΔW dissipated during each loading cycle was defined as the hysteresis area of the stress-strain relationship (Kokusho 2014 among others), and its total amount $\Sigma\Delta W$ was evaluated as the sum. In order to compare the accumulation rate of the dissipated energy among different test results, the accumulated shear strain $\Sigma\gamma$ was evaluated as the sum of the single shear strain amplitude during the cyclic loading stage, as illustrated in Fig. 6b. As a result, their relationship could be obtained as typically shown in Fig. 6c.

In Fig. 7a, the relationships between $\Sigma\Delta W$ and $\Sigma\gamma$ in the first liquefaction stage at the relative density of 51 to 54 % were compared among the tests with different γ_{DAmax} values in the range of 0.2 % and 10.0 %. Naturally, the amounts of both $\Sigma\Delta W$ and $\Sigma\gamma$ increased with the increase in the γ_{DAmax} values, while their relationships were almost identically overlapped to each other. This overlap confirms high repeatability of the test results.

The stress path and stress-strain relationships during the first liquefaction stage in the test with γ_{DAmax} =5.0 % are shown in Fig. 7b and 7c, respectively, on which the following three characteristic states are marked; the stress path first reached the phase transformation line (denoted as PTL hereafter) at state 1; the shear strain amplitude started to increase rapidly after passing state 2; and the vertical stress became almost zero for the first time at state 3.

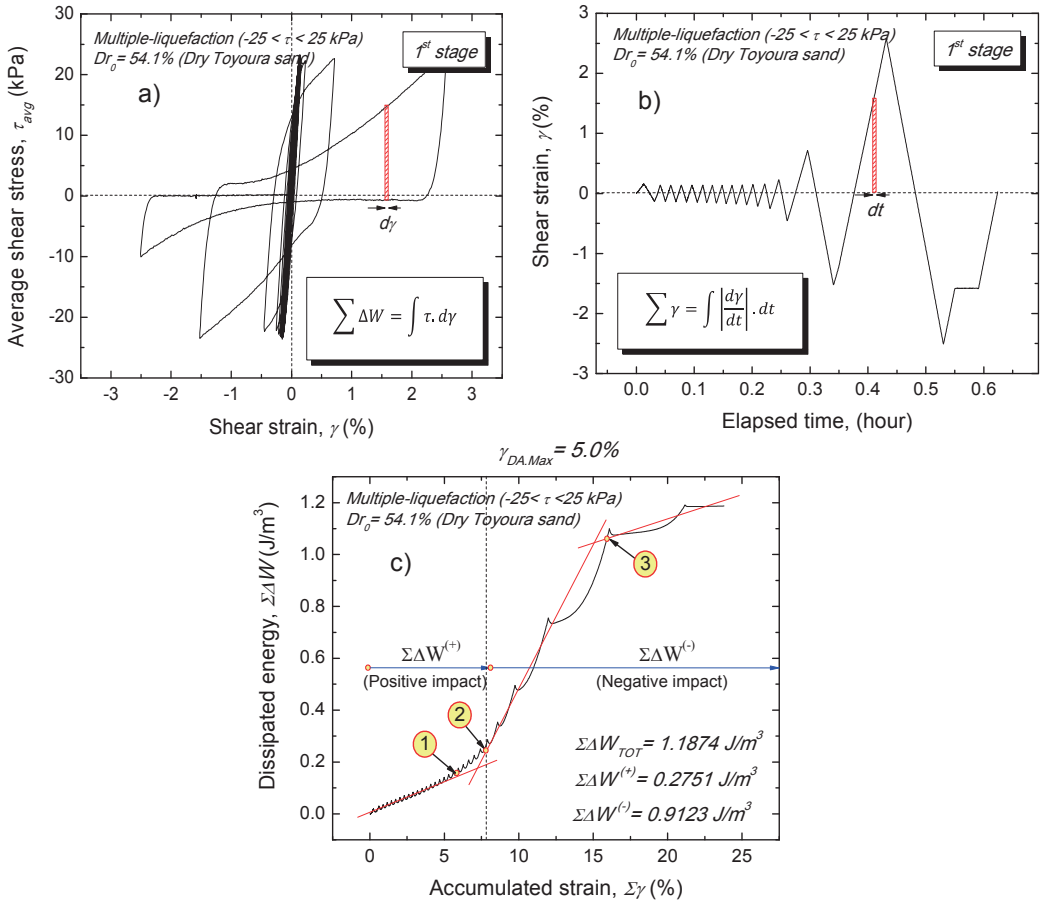

Figure 6. Definition of a) dissipated energy and b) accumulated shear strain, and c) their typical relationship

In the corresponding figures (i.e., the relationship between $\Sigma\Delta W$ and $\Sigma\gamma$ as shown in Fig. 6c and the relationship between the vertical stress and $\Sigma\gamma$ as shown in Fig. 7d), the location of the above three states are also marked. From these figures, the following trends of behavior could be observed:

1) Until reaching state 1, the value of dissipated energy $\Sigma\Delta W$ increased linearly with the accumulated strain $\Sigma\gamma$.
2) After passing state 1, the accumulation rate of $\Sigma\Delta W$ became higher than the above linear trend. On the other hand, the reduction rate of the vertical stress relative to $\Sigma\gamma$ did not change largely.
3) After passing state 2, the relationship between $\Sigma\Delta W$ and $\Sigma\gamma$ entered into the second linear region with higher accumulation rate of $\Sigma\Delta W$, which was accompanied by remarkable cyclic mobility (i.e., temporary recovery of vertical stress, as can be seen in Fig. 7d).
4) After passing state 3, the $\Sigma\Delta W$ and $\Sigma\gamma$ relationship changed again, entering into the third linear region with lower accumulation rate of $\Sigma\Delta W$.

In summary, as illustrated in Fig. 7a, the above three linear regions that appeared in the $\Sigma\Delta W$ and $\Sigma\gamma$ relationship can be linked to the following three steps; in Step-I, within the region where the stress path does not intersect with the PTL, contraction takes place; in Step-II, the stress path passes the PTL, and thus dilation starts to be mobilized partly; and in Step-III, the stress path reaches the zero vertical stress state (i.e., the initial liquefaction state), and consequently large shear deformation develops.

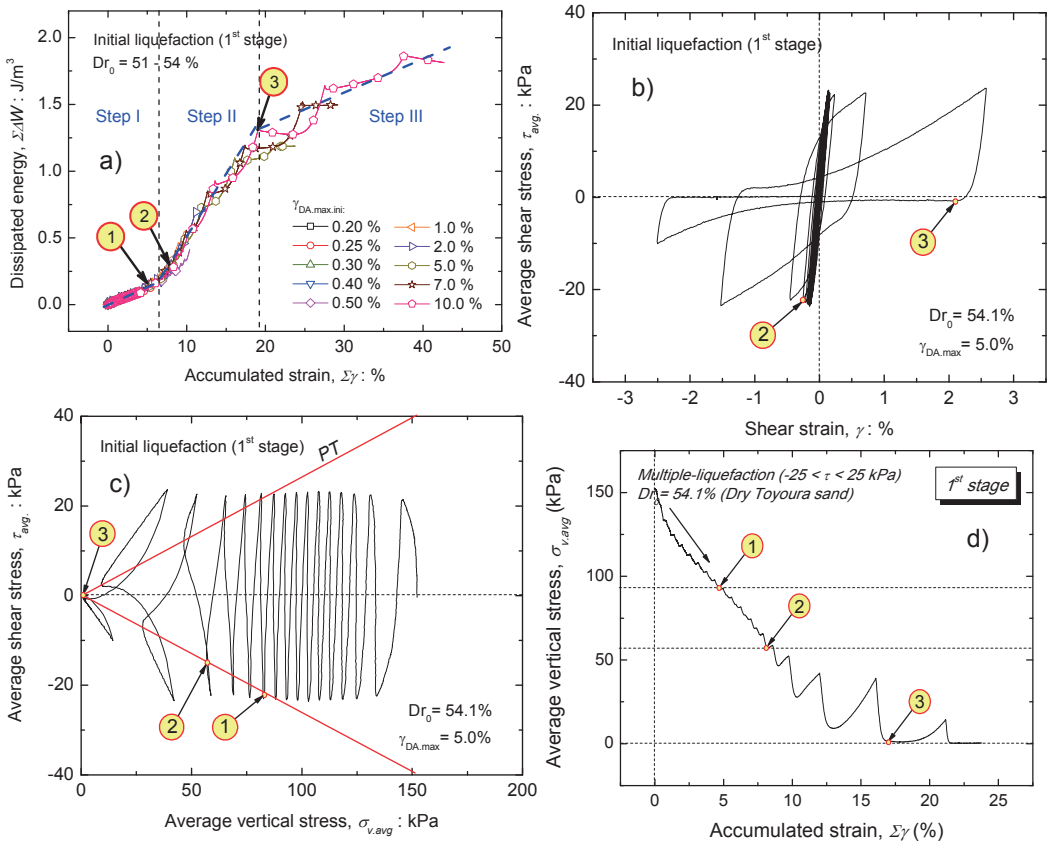

Figure 7. a) Relationships between dissipated energy and accumulated shear strain in the 1st liquefaction stage, and typical test result; b) stress path, c) stress-strain relationship and d) relationship between vertical stress and accumulated shear strain

Effects of dissipated energy on re-liquefaction behavior

In Fig. 8, the relationship between the energy $\Sigma\Delta W^{(1st)}$ that was dissipated during the first liquefaction stage and the number of cycles $N_L^{(2nd)}$ that was required to induce the double amplitude shear strain of 2 % in the second liquefaction stage are shown, on which the boundaries between the three steps as introduced in the previous section are also indicated. For comparison, test results on the "pre-sheared" specimens are also plotted in terms of the relationship between $\Sigma\Delta W$ dissipated during the pre-shearing stage and N_L in the subsequent (i.e., first) liquefaction stage, where the pre-shearing history was applied to the specimen by conducting in advance drained cyclic loading at a double amplitude shear strain of 0.2 % with the specified number of cycles in the range of 5 to 1000. From this figure, following observations can be made:

1) When the dissipated energy was smaller than about 0.2 J/m^3 (i.e., in Step-I for the first liquefaction stage), the two relationships derived from different test series were almost similar to each other. This similarity suggests that the dissipated energy in the preceding liquefaction or pre-shearing stage is one of the key parameters that affect the liquefaction resistance to be mobilized in the next stage.
2) When the dissipated energy exceeded the above threshold, the two relationships were very different from each other. This discrepancy was possibly caused by the dilation mobilized during the first liquefaction stage (i.e., in Step-II and Step-III), which was not mobilized during the pre-shearing stage conducted at limited amount of shear strain amplitude (γ_{DA}=0.2 %).

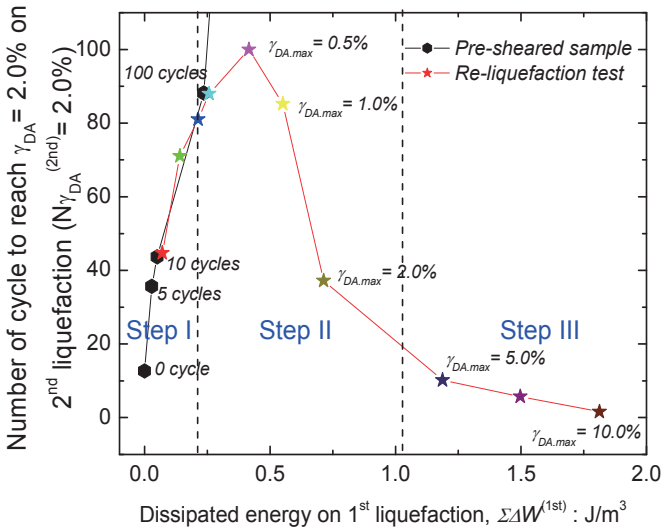

Figure 8. Relationships between dissipated energy in the 1st liquefaction stage and number of cycle in the 2nd liquefaction stage

3) Regarding the re-liquefaction resistance, the $N_L^{(2nd)}$ value was largest in the test with γ_{DAmax} =0.5 %. Such response can be explained by assuming two opposite impacts of the dissipated energy; even in Step-II, the re-liquefaction resistance tended to increase due to a positive impact which can be inferred from the N_L and $\Sigma\Delta W$ relationship obtained with pre-sheared specimens; in addition, due possibly to the effect of dilation as discussed above, an opposite impact to reduce the re-liquefaction resistance started to accumulate rapidly in Step-II, which continued to accumulate in Step-III; as a combination of these two impacts, the re-liquefaction resistance became largest in the course of Step-II.

Based on the above analysis, it can be inferred that the energy dissipated during the first liquefaction stage exhibited both positive and negative impacts. A positive impact of dissipated energy to cause increase in the re-liquefaction resistance accumulated in Step-I, in a manner that was similar to the cases with "pre-sheared" specimens. On the other hand, a negative impact of dissipated energy prevailed in Step-II and Step-III, which resulted in reduction of the re-liquefaction resistance.

Evaluation of re-liquefaction resistance based on dissipated energy in previous liquefaction stage

The $\Sigma\Delta W$ and $\Sigma\gamma$ relationships in the first to fifth liquefaction stages for the test with γ_{DAmax} =5.0 % are shown in Fig. 9. During each of the liquefaction stages except for the sixth one, the accumulation rate of the dissipated energy changed twice, exhibiting the same behavior categorized before as Step-I, Step-II and Step-III for the first liquefaction stage. The cyclic loading in the sixth stage may have been terminated before reaching Step-III, resulting into only a single change in the accumulation rate of the dissipated energy in-between Step-I and Step-II.

It can be also noticed from Fig. 9 that the dissipated energy in Step-I and Step-III, respectively, accumulated at similar rates irrespective of the different liquefaction stages, while the dissipated energy in Step-II tended to accumulate at a lower rate during later stages of liquefaction. In addition, the shift from Step-I to Step-II occurred at smaller values of the dissipated energy in the earlier (i.e., first and second) liquefaction stages, and then these threshold values of the dissipated energy increased with the liquefaction stages. In another word, the region of Step-I expanded in general with the liquefaction stages.

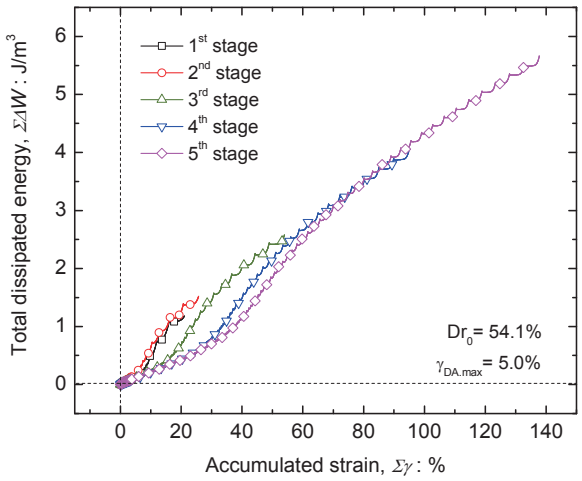

Figure 9. Relationships in the 1st to the 5th liquefaction stages with γ_{DAmax} =5.0 %

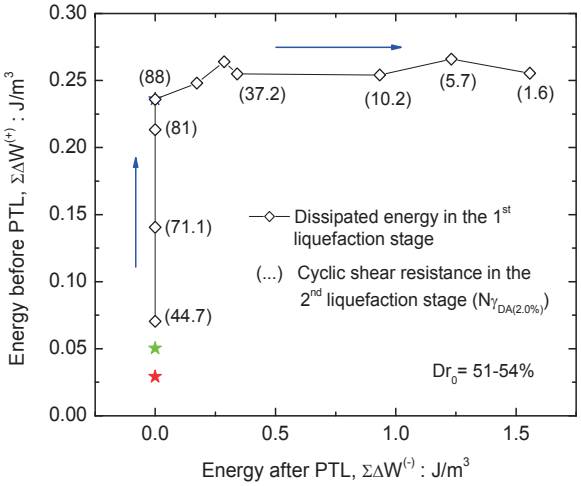

Figure 10. Relationships between positive and negative impacts of dissipated energy during the 1st liquefaction stage and the pre-shearing stage with 5 and 10 cycles

It should be noted that, as shown in Fig. 4b, the N_L values increased also with the liquefaction stages for the test with γ_{DAmax} =5.0 %, except for its reduction in-between the first and second liquefaction stages. Such similarity between the expansion of the Step-I region and the increase in the re-liquefaction resistance may be linked with the effects of the dissipated energy on the re-liquefaction behavior as discussed in the previous section. As illustrated in Fig. 6c, therefore, a positive impact of dissipated energy $\Sigma\Delta W^{(+)}$ was assumed for simplicity to accumulate only until reaching the state 2 as defined before, while its negative impact $\Sigma\Delta W^{(-)}$ was assumed to accumulate after exceeding this state. This state 2 was selected as the threshold, since it was attained immediately after shifting from Step-I to Step-II as shown in Fig. 7a.

Based on these assumptions, the positive and negative impacts of the dissipated energy during the first liquefaction stage and the pre-shearing stage with 5 and 10 cycles for the test cases shown in Fig. 8 were evaluated and plotted in Fig. 10. The N_L values obtained in the next liquefaction stage were

also depicted in the figure. Without any negative impact (i.e., while keeping $\Sigma\Delta W^{(-)}=0$), the re-liquefaction resistance increased with the positive impact $\Sigma\Delta W^{(+)}$. After $\Sigma\Delta W^{(+)}$ reached a peak value of around 0.25 J/m^3, accumulation of $\Sigma\Delta W^{(-)}$ started, which was in general accompanied with reduction in the re-liquefaction resistance. Only at the beginning of accumulation of $\Sigma\Delta W^{(-)}$, the re-liquefaction resistance increased (i.e., the N_L value increased from 88 to 100), due to the difference in the amounts of dissipated energy at the state 2 employed as the threshold and for the test with γ_{DAmax} =0.5 % that exhibited the largest re-liquefaction resistance (Fig. 8).

By adopting the same assumptions as above, the values of $\Sigma\Delta W^{(+)}$ and $\Sigma\Delta W^{(+)}$ for the test results from the subsequent liquefaction stages were also evaluated and plotted in Fig. 11a, together with the N_L values obtained in the next liquefaction stage. From this figure, following observations can be made:

1) In general, both of the amounts of ΣΔW(+) and ΣΔW(-) increased with the liquefaction stage.
2) For each of the subsequent liquefaction stages (i.e., except for the first liquefaction stage), the amount of ΣΔW(+) decreased with the increase in ΣΔW(-), accompanied by the reduction in the N_L values.
3) By associating the test data that exhibited similar NL values irrespective of the liquefaction stage, rather unique relationships among the amounts of ΣΔW(+) and ΣΔW(-) that accumulated in the previous liquefaction stage and the liquefaction resistance that was mobilized in the next stage could be obtained, as typically drawn in Fig. 11a for the N_L values equal to 10, 30, 50 and 100.

A close-up of Fig. 11a for relatively small values of $\Sigma\Delta W^{(+)}$ and $\Sigma\Delta W^{(-)}$ is shown in Fig. 11b. It can be confirmed that the above unique relationships are also valid in this region. Such uniqueness implies that evaluation of the positive and negative impacts of dissipated energy during the immediate-past liquefaction event would enable us to predict the liquefaction properties in the next event. By analyzing the strong motion records obtained in the liquefied zones, for example, we may be able to evaluate these impacts.

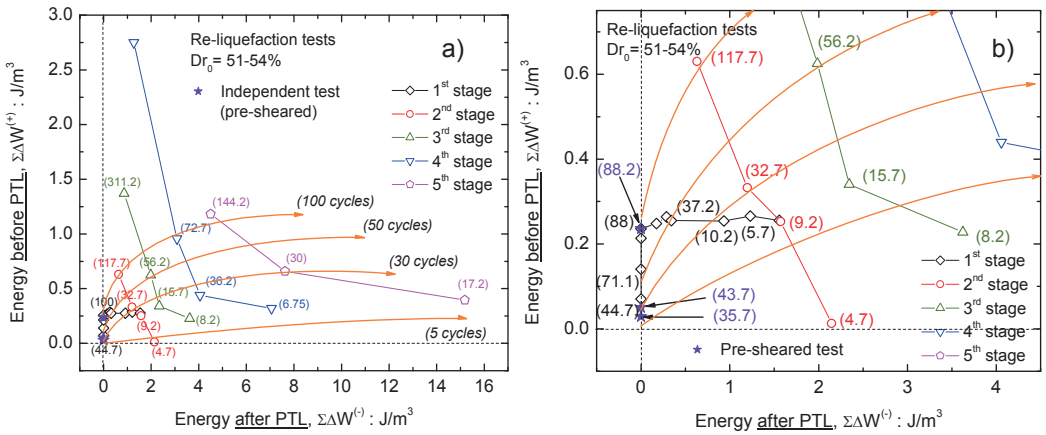

Figure 11. a) Relationships among positive and negative impacts and the number of cycles in the next liquefaction stage, and b) its close-up around the origin

CONCLUSIONS

The following main conclusions can be drawn from the analysis of dissipated energy conducted on results from a series of constant-volume cyclic torsional shear tests on Toyoura sand subjected to various strain amplitudes using stacked-ring shear apparatus:

1) During liquefaction, the accumulation of dissipated energy can be divided into three steps that correspond to specific stress states. In Step-I, within the region where the stress path does not

intersect with the phase transformation line, PTL, contraction takes place. In Step-II, the stress path passes the PTL, and thus dilation starts to be mobilized partly. In Step-III, the stress path reaches the zero vertical stress state (i.e., the initial liquefaction state), and consequently large shear deformation develops.

2) The amount of dissipated energy in the previous liquefaction stage significantly affects the behavior in the next liquefaction stage. The energy dissipated during the previous stage can exhibit both positive and negative impacts. A positive impact of dissipated energy ($\Sigma\Delta W(+)$) accumulates in Step-I before the stress path passes the PTL. In Step-II and Step-III, on the other hand, a negative impact of dissipated energy ($\Sigma\Delta W(-)$) prevails. A larger amount of $\Sigma\Delta W(+)$ results in a higher liquefaction resistance in the next stage, while a larger amount of $\Sigma\Delta W(-)$ causes an opposite impact.
3) Compilation of all re-liquefaction test results under various strain amplitudes revealed unique relationships among the amounts of $\Sigma\Delta W(+)$ and $\Sigma\Delta W(-)$ that accumulate in the immediate-past liquefaction stage and the liquefaction resistance to be mobilized in the next stage.

REFERENCES

Ishihara, K., and Okada, S. (1978): "Effects of stress history on cyclic behavior of sand", *Soils and Foundations*, 18(4), 31-35.

Kokusho, T. (2014): "Liquefaction potential evaluations: energy-based method versus stress-based method", *Canadian Geotechnical Journal*, 50, 1088-1099.

Wahyudi, S., Koseki, J. and Sato, T. (2014): "Characteristics of re-liquefied behavior of sand by means of image analysis using stacked-rings shear apparatus", *Bulletin of ERS*, 47, 15-26.